



Source versus weathering processes as controls on the Mackenzie river uranium isotope signature

Quentin Charbonnier^{a,b,*}, Matthew O. Clarkson^a, Robert G. Hilton^c, Derek Vance^a

^a Department of Earth Sciences, ETH Zürich, Clausiusstrasse 25, 8092 Zürich, Switzerland

^b Université de Paris, Institut de physique du globe de Paris, CNRS, 75005 Paris, France

^c Department of Earth Sciences, University of Oxford, Oxford OX1 3AN, United Kingdom

ARTICLE INFO

Editor: Christian France-Lanord

Keywords:

Weathering

Mackenzie Basin

Uranium stable isotopes

ABSTRACT

Uranium (U) isotope signatures ($\delta^{238}\text{U}$) recorded in sedimentary archives provide insight into the paleo redox state of the ocean. But the robust interpretation of these sedimentary U isotope records requires characterisation of the U isotope signature of rivers, the main source of U to the ocean. The main controlling factors on riverine $\delta^{238}\text{U}$ remain poorly constrained. Here, we investigate the elemental and isotope signatures of uranium in the dissolved and solid loads of a well-characterised river, the Mackenzie Basin (Canada).

In the Mackenzie Basin, the solid load $\delta^{238}\text{U}$ shows a positive relationship with U and vanadium (V) contents, consistent with the suggestion that particulate $\delta^{238}\text{U}$ are explained by variable contributions via erosion of silicate and black shale. The $\delta^{238}\text{U}$ of the dissolved and solid loads are correlated which, at first sight, suggests no U isotope fractionation during chemical weathering, and a purely lithological control on both the river dissolved and solid $\delta^{238}\text{U}$. Moreover, relationships between dissolved U and $\delta^{238}\text{U}$ and major elements such as calcium and sulfate, also support the idea of a lithological control. However, the $\delta^{238}\text{U}$ of end members inferred from mixing relationships are not consistent with binary mixing of two sources, suggesting some potential U isotope fractionation during weathering. In fact, the abundance of U in the river dissolved load is always lower than that predicted by silicate rock weathering. This suggests that 1) the weathering of silicate only can explain the abundance of U in the river dissolved load and 2) secondary weathering processes scavenge a proportion of the U released by primary mineral breakdown. The broad negative relationship between $\delta^{238}\text{U}$ and the depletion of dissolved U is also consistent with the control of dissolved $\delta^{238}\text{U}$ by secondary weathering processes following silicate mineral breakdown. The relationships observed between dissolved U, $\delta^{238}\text{U}$ and the large-scale environmental controls on weathering processes (such as weathering intensity or runoff) support this hypothesis.

Overall, our interpretations of the variation in the river dissolved $\delta^{238}\text{U}$ challenge the common assumption of the control of dissolved U by black shale and carbonate weathering. In addition, we suggest that the extent of secondary weathering processes can imprint on the U isotope signature of rivers, now and in the past.

1. Introduction

Uranium (U) and its isotopes have been extensively used to constrain a wide range of processes in Earth sciences. The U isotope series (and associated daughter nuclides) including the $^{234}\text{U}/^{238}\text{U}$ ratio have been shown to provide insight into timescales and rates of weathering and erosion processes (Chabaux et al., 2003). More recently, “stable” U isotope ratios ($^{238}\text{U}/^{235}\text{U}$, reported as $\delta^{238}\text{U}$) have been recognised as a tool to reconstruct the extent of oceanic anoxia in the Earth’s past (see the review of Andersen et al., 2017 and e.g., Weyer et al., 2008; Montoya-Pino et al., 2010; Brennecka et al., 2011a; Asael et al., 2013;

Kendall et al., 2013; Dahl et al., 2014; Kendall et al., 2020), due to the preferential incorporation of the heavier ^{238}U isotope into the solid phase (Stirling et al., 2007; Weyer et al., 2008; Brown et al., 2018). The application of this paleo-redox proxy must rest on a sound understanding of the U cycle (Andersen et al., 2017), particularly the patterns and controls of the $\delta^{238}\text{U}$ values of riverine inputs to the oceans. Modern riverine catchments, and the weathering and erosion processes which are imprinted on the geochemical composition of their particulate and dissolved loads offer a way to better understand this input vector in the past (Gaillardet et al., 1999b).

Previous studies on the concentrations of dissolved U in rivers

* Corresponding author at: Department of Earth Sciences, ETH Zürich, Clausiusstrasse 25, 8092, Zürich, Switzerland.

E-mail address: quentin.charbonnier@erdw.ethz.ch (Q. Charbonnier).

around the world have emphasised the dominant role of carbonate and black shale weathering in driving the riverine dissolved U flux (e.g., Sarin et al., 1990; Palmer and Edmond, 1993; Dunk et al., 2002). However, the variability in the $\delta^{238}\text{U}$ of the dissolved load of rivers (from -0.72‰ to $+0.06\text{‰}$; Andersen et al., 2015; Tissot and Dauphas, 2015; Andersen et al., 2016; Noordmann et al., 2016) is less well understood. The large variability (for a heavy mass isotope system) ranges above and below the average silicate $\delta^{238}\text{U}$ value of $-0.29 \pm 0.03\text{‰}$, measured on various igneous and sedimentary rock types (Telus et al., 2012; Andersen et al., 2015; Tissot and Dauphas, 2015; Andersen et al., 2016; Noordmann et al., 2016). The measurements to date imply that different sources and/or fractionation mechanisms must shift dissolved U isotope signatures of rivers towards heavier or lighter values (Andersen et al., 2016). However, we still lack clarity on the factors that controls these shifts away from rocks in riverine dissolved loads (Tissot and Dauphas, 2015; Andersen et al., 2016; Noordmann et al., 2016). In particular, small rivers have been shown to exhibit greater U isotope variability, consistent with either a lithological control or fractionation during chemical weathering (Noordmann et al., 2016). On a larger scale, rivers with lower dissolved U flux (such as the Nile or Kalix) show dissolved $\delta^{238}\text{U}$ values that are higher than silicates, which could be consistent with the preferential sequestration of light U isotopes into residual solids during weathering (Holmden et al., 2015; Andersen et al., 2016). On the other hand, the dissolved $\delta^{238}\text{U}$ of some rivers, such as the Yangtze or Indus, may display a lithological control due to the significant contributions from black shale and/or carbonate/evaporite weathering (Andersen et al., 2016; Noordmann et al., 2016). Given the variability observed in the modern dissolved load of rivers, riverine $\delta^{238}\text{U}$ may have changed through Earth history, with implications for oceanic isotope mass balance. Indeed, different riverine U isotope compositions have been inferred to help explain ancient seawater $\delta^{238}\text{U}$ reconstructions from carbonates (Lau et al., 2016; Clarkson et al., 2018). Without some understanding of the controls on the modern variability, it is difficult to assess the extent to which changes in the past could be important for oceanic mass balance.

In this contribution, we explore these controlling factors using a dataset of river dissolved and solid loads from a well-characterised river in terms of major elements as well as radiogenic and stable isotope systems (Vigier et al., 2001; Millot et al., 2003; Huh et al., 2004; Lemarchand and Gaillardet, 2006; Calmels et al., 2007; Millot et al., 2010; Tipper et al., 2012; Dellinger et al., 2021; Charbonnier et al., 2022): the Mackenzie Basin (north Canada). The variable amount of carbonate, silicate and black shale that make up the Mackenzie Basin bedrock provides a useful geological framework to assess source rock influence on dissolved $\delta^{238}\text{U}$ (Millot et al., 2003; Huh et al., 2004). Additionally, the gradient in weathering regime across the Mackenzie Basin (Lemarchand and Gaillardet, 2006; Millot et al., 2010) can be used to investigate the importance of secondary weathering processes on the dissolved $\delta^{238}\text{U}$. Our data suggest that, while dissolved $\delta^{238}\text{U}$ in the Mackenzie Basin show an apparent source control, the inferred lithological end members cannot explain all of the isotope variability. We also observe a distinct U depletion associated with variation of $\delta^{238}\text{U}$ in the dissolved load compared to estimates for the bedrock, identifying an important U removal process in the weathering environment, potentially through the formation of secondary phases. More broadly, this suggests that riverine $\delta^{238}\text{U}$ could have changed in tandem with changes in the weathering regime on geological timescales.

2. Materials and methods

2.1. The Mackenzie Basin

2.1.1. The geological setting of the Mackenzie Basin

The broad characteristics of the Mackenzie Basin (Fig. 1) have been extensively described in previous studies (Reeder et al., 1972; Carson et al., 1998; Millot et al., 2003). Briefly, the Mackenzie Basin drains

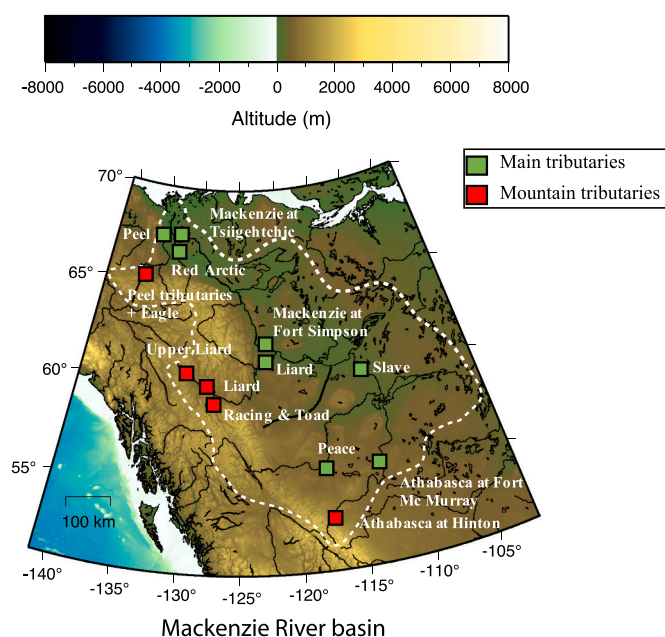


Fig. 1. Map of the Mackenzie Basin with the sampling locations from this study. The mountain tributaries drain the most elevated part of the Mackenzie Basin and correspond to the headwater catchments of the main rivers. The main tributaries drain larger areas, including the mountainous region as well as the Interior Platform (the central part of the Basin). The Mackenzie at Tsiigehtchic sampling site corresponds to the mouth of the Mackenzie Basin. Map modified from Dellinger et al. (2014).

around $1.8 \times 10^6 \text{ km}^2$ and has an annual discharge of $308 \text{ km}^3/\text{yr}$. The climate is cold on average (4°C), and the amount of precipitation increases across the basin from the east (250 to 400 mm/yr) to the west (1000 to 1500 mm/yr). Similarly, erosion rates show a positive gradient from the east (flattest part of the basin) to the west (mountainous part of the basin). The Mackenzie Basin can be split into three different geological units from the east to the west (Millot et al., 2003). First, the Canadian Shield is made up of old Precambrian craton and metamorphic rocks, such as granitic gneiss and schists. Second, the Interior Platform, corresponding to the central part of the basin, is underlain by sedimentary rocks aged from Cambrian to Cretaceous, including sandstone, shale, black shale, carbonate and evaporite. Third, the Mackenzie Mountains, located in the western part of the basin, corresponds to a tectonically active margin. Most of the Mackenzie Mountains is formed by sedimentary rocks from the Proterozoic to the Mesozoic, such as limestone, dolomite, shale and black shale, with rare intrusions of igneous rocks.

In this study, U isotope data are reported for rivers draining 1) the Mackenzie Mountains only: the Racing, Toad, Upper Liard, Athabasca at Hinton, Eagle, Ogilvie, Blackstone and 2) the main Mackenzie tributaries that drain both the Mackenzie mountains and the Interior Platform, such as the Mackenzie main channel (at Fort Simpson and Tsiigehtchic), Peel, Red Arctic, Athabasca at Fort Mac Murray, Liard, Slave, Peace. Uranium abundances in the rivers draining the Canadian Shield were too low (0.1 or less $\mu\text{g/L}$ of U) to perform stable U isotope ratio measurements, given the amount of water sample available (around 100 mL).

2.1.2. Previous studies of major cations and Sr isotopes

Previous studies of the same samples investigated here for $^{238}\text{U}/^{235}\text{U}$ have presented major element, radiogenic strontium and osmium isotope ratios, and various stable isotope ratios, such as boron (B), lithium (Li), magnesium (Mg), sulfate-oxygen system (S, O), barium (Ba), rhenium (Re) (Millot et al., 2003; Huh et al., 2004; Lemarchand and Gaillardet, 2006; Calmels et al., 2007; Millot et al., 2010; Horan

et al., 2020; Dellinger et al., 2021; Charbonnier et al., 2022) and $^{234}\text{U}/^{238}\text{U}$ ratio data (Vigier et al., 2001). The findings from these previous papers are briefly summarised here. The major cations show very different degrees of variance (Millot et al., 2003). Sodium ranges over more than an order of magnitude (from 30 to 619 $\mu\text{mol/L}$), whereas potassium (K) is less abundant and relatively constant in concentration (around 20 $\mu\text{mol/L}$, on average). Overall, the concentrations of these two alkali metals increase from the Mackenzie Mountains to the Interior Platform/Lowland (Millot et al., 2003). In contrast, calcium (Ca) and magnesium (Mg) concentrations are more homogeneous and dominate the cation load (Millot et al., 2003). Sulfate concentrations (SO_4) show an inverse pattern to Na, with higher concentrations in the Mackenzie Mountains and a decrease in the Lowland.

The different contributions from silicate, carbonate and evaporite weathering and sea-salt input have been computed in Millot et al. (2003). Evaporite dissolution and sea-salt contribution have a minor influence on the dissolved load of the Mackenzie Basin tributaries (Millot et al., 2003; Calmels et al., 2007). The sea salt contribution accounts for only a few percent of the total dissolved Na inventory - as shown by the excess of Na compared to the evaporite and sea-salt Na/Cl ratios - and is almost negligible for other major cations (<1% of the total cationic load; Millot et al., 2003). Regarding evaporites, halite dissolution accounts for 50% of the dissolved Na in the Mackenzie main stem only and is much less significant for other tributaries (between 0 and 20%) - <1 % of the total cationic load (Millot et al., 2003). Similarly, gypsum dissolution has a minor influence on the dissolved load of the Mackenzie Basin tributaries (Calmels et al., 2007), accounting for between 0 and 20% of the dissolved SO_4 across the Mackenzie tributaries, except for the Mackenzie main tributary at Fort Simpson (30%) and the Athabasca at Hinton (61%). Assuming that gypsum is a pure Ca-phase (CaSO_4), its dissolution cannot contribute >10% of the total Ca dissolved load, except for the Athabasca at Hinton (27%). The contribution of silicate weathering is retrieved using the Na corrected for sea-salt and evaporite input (or Na^*). This correction is performed using the Na/Cl ratios of sea salt and evaporite and the dissolved Cl concentrations (Millot et al., 2003). All rivers show a strong excess of dissolved Ca compared to the Ca/Na ratio of silicate ($\text{Ca}/\text{Na}^* \approx 0.3$; Gaillardet et al., 1999b), an observation that has been attributed to the dominant influence of carbonate weathering on the dissolved load chemistry in the Mackenzie Basin (Millot et al., 2003). Thus, almost all of the Ca (and Mg) derives from carbonate weathering in the Mackenzie Basin (Millot et al., 2003). The weathering of carbonate is fuelled by carbonic acid as well as sulfuric acid produced by sulfide oxidation hosted in black shales (Calmels et al., 2007). Altogether, these previous studies show that a range of different lithologies contribute to the Mackenzie Basin river chemistry.

2.2. Sampling procedure

The samples derive from a number of sampling campaigns performed by the Institut de Physique du Globe de Paris (IPGP) (CAN96, CAN99, CAN09, CAN10) and Durham University (CAN13) (Vigier et al., 2001; Millot et al., 2003; Lemarchand and Gaillardet, 2006; Tipper et al., 2012; Dellinger et al., 2014; Horan et al., 2019; Horan et al., 2020; Charbonnier et al., 2022). The samples of river waters were filtered at 0.2 μm on-site using Teflon-lined filtration units and stored in pre-washed polypropylene bottles. The river water samples were acidified to $\text{pH} \approx 2$ with ultra-pure HNO_3 and stored in a cold room. River sediments are sorted in the water column of large rivers. The finest river sediments are carried in surface water, while the coarsest sediments are transported near the bottom (Bouchez et al., 2011). For this reason, river sediments have been sampled at a range of depths in some of the main Mackenzie tributaries (Dellinger et al., 2014). River suspended sediments were recovered from the filter by either scraping or rinsing the filter with the filtered river water (see above), while the river bed sediments were taken from the bottom of the river channel using a bucket.

The river sediments were dried in the lab at 50 °C or by freeze-drying and subsequently crushed using an agate mortar (Dellinger et al., 2014). For isotope analyses, a mass of 50 to 100 mg of sediment powder was digested with HNO_3 -HF in a Teflon bomb at 130 °C. The solution was then dried down and the solid was taken up into HCl to re-dissolve fluorides. This step was repeated until the total dissolution of fluorides was achieved. The solution was eventually diluted with HCl 0.6 M in a volume of 10 mL (Dellinger, 2013).

2.3. Elemental abundance and isotopes ratio determination

The dissolved concentration of major elements used here come from Millot et al. (2003) and Horan et al. (2020) as outlined in section 2.1.2. Concentrations of major cations and anions were measured using ion chromatography (Dionex 300). The reproducibility was better than 5% (2 S.D.). The dissolved uranium concentration was measured using ICP-MS. Concentrations for major and trace elements in river sediments were measured using ICP-AES and ICP-MS, after alkali fusion, at the SARM (Service d'analyse des Roches et des minéraux, INSU facility, Vandoeuvre les Nancy, France). Uncertainties were lower than 3% for major elements and lower than 10% for trace elements.

The chemical separation of U and the measurement of its isotope ratios were carried out at the Institute of Geochemistry and Petrology, ETH Zürich. The chemical separation protocol comes from Bura-Nakić et al. (2018) and Clarkson et al. (2020). In order to get a minimum of 10 ng of U, an aliquot of sample (between 50 and 120 mL of river water or a few mg of digested river sediment) was spiked with IRMM-3636 U double spike (aiming for $^{236}\text{U}/^{235}\text{U} \sim 4$) and dried down over 12 to 20 h (depending on the sample volume). The sample was taken up in 1 M HCl and loaded in a 200 μL column containing cleaned Re-Resin (Trisken Technologies). Matrix was eluted using 4 mL of 1 M HCl followed by 2 mL of 0.2 M HCl. Uranium was then eluted using 2 mL of 0.2 M HCl + 0.3 M HF. Prior to analysis, the samples were processed via overnight treatment with concentrated HNO_3 and H_2O_2 to oxidize organic residue from the resin elution. Uranium isotope ratio measurements were performed using an MC-ICPMS (Neptune Plus) from Thermo-Finnigan. The generally low amount of U in our samples required the use of a desolvating nebulizer (Aridus II CETAC) with 'Jet + X cones' to increase ion beam intensities in low U concentration samples. Depending on the amount of uranium available, the samples and standards were run at concentrations between 20 and 40 $\mu\text{g/L}$ of uranium, giving an intensity range between 20 and 40 V for ^{238}U . Instrument protocols are extensively described in Andersen et al. (2015). Uranium $^{238}\text{U}/^{235}\text{U}$ isotope ratios are reported relative to the standards CRM-145 = 0‰, and secular equilibrium for $^{234}\text{U}/^{238}\text{U}$:

$$\delta^{238}\text{U} = \left[\frac{^{238}\text{U}/^{235}\text{U}_{\text{sample}}}{^{238}\text{U}/^{235}\text{U}_{\text{CRM-145}}} - 1 \right] \times 1000 \quad (1)$$

$$\delta^{234}\text{U} = \left[\frac{(^{234}\text{U}/^{238}\text{U})_{\text{sample}}}{(^{234}\text{U}/^{238}\text{U})_{\text{sec.eq}}} - 1 \right] \times 1000 \quad (2)$$

The external reproducibility and accuracy were determined through the repeated measurement of a secondary standard: CZ-1 (uraninite) yielding a $\delta^{238}\text{U}$ of $-0.04 \pm 0.05\%$ ($n = 25$; 2SD), matching well with the previously reported value (Andersen et al., 2015; Andersen et al., 2016; Bura-Nakić et al., 2018; Clarkson et al., 2020; Li and Tissot, 2023). The lower signals obtained for some samples lead to internal errors larger than long-term reproducibility of the CZ-1. In this case, the internal errors are taken to represent the uncertainty.

3. Results

The data for the river dissolved and solid loads are reported in Tables 1 and 2 (see Supplementary tables), respectively. Measured concentrations of dissolved U are similar to those reported previously for the Mackenzie (Vigier et al., 2001) and vary from 1.26 (Mackenzie at Fort Simpson) to 7.3 nmol/L (Ogilvie), with an average of 3 nmol/L

(Table 1; Fig. 2). This range is consistent with results previously reported for small and large rivers globally (a maximum of a few nmol/L; Palmer and Edmond, 1993; Dunk et al., 2002; Andersen et al., 2016; Noordmann et al., 2016). The concentration of dissolved U shows a similar range in the main tributaries and the Mackenzie Mountain tributaries. No relationship is observed between dissolved uranium and sodium deriving from silicate weathering (Na^* ; corrected for the sea-salt and evaporite inputs using the measured Cl concentration and the Na/Cl ratio of seawater; Fig. 2a). Uranium and Ca concentrations show a positive trend for most samples (Fig. 2b), though three (CAN09–51, CAN13–05 and CAN13–14) lie significantly off it to higher Ca. A similar trend is observed between U and SO_4 (Fig. 2c), again with samples CAN13–05 and CAN13–14 and CAN09–51 as outliers lying towards high SO_4 . A relationship is observed between dissolved U and alkalinity (HCO_3 ; Fig. 2d), including the aforementioned outliers.

Riverine dissolved $\delta^{238}\text{U}$ exhibits significant variations (from $-0.15 \pm 0.05\text{‰}$ to $-0.39 \pm 0.05\text{‰}$) with an average value of -0.24‰ , within the range previously reported for other rivers (from $+0.06$ to -0.72‰ ; Andersen et al., 2016; Noordmann et al., 2016) and close to that for silicate rocks ($-0.29 \pm 0.03\text{‰}$; Tissot and Dauphas, 2015). Dissolved $\delta^{238}\text{U}$ does not show a significant difference between the main tributaries and the Mackenzie Mountains tributaries. Overall, $\delta^{238}\text{U}$ values are not well correlated with major ion concentrations, albeit with a pattern suggesting a positive trend with Na^* (excluding CAN13–05 that has a lower $\delta^{238}\text{U}$ value) (Fig. 2e–h). Dissolved $^{234}\text{U}/^{238}\text{U}$ isotope ratios (Table 1, Vigier et al., 2001) do not correlate with $\delta^{238}\text{U}$ (not shown), consistent with global observations (Tissot and Dauphas, 2015; Andersen et al., 2016).

Uranium abundances in river sediments vary from 1.5 to 4 mg/kg (Table 2), the average of 3.2 mg/kg being identical to typical values for silicate rocks forming the continental crust (around 3 mg/kg; Taylor and McLennan, 1995; Rudnick and Gao, 2013). River sediment $\delta^{238}\text{U}$ range from $-0.14 \pm 0.05\text{‰}$ to $-0.34 \pm 0.05\text{‰}$ with an average of -0.23‰ (Fig. 3a), slightly higher than average silicate rocks ($-0.29 \pm 0.03\text{‰}$; Tissot and Dauphas, 2015). Overall, the $\delta^{238}\text{U}$ of river sediments are broadly similar to their river dissolved $\delta^{238}\text{U}$ (Fig. 3b).

4. Discussion

Overall, dissolved uranium and its isotopes are not strongly correlated with major elements. On the other hand, the overall variability in dissolved $\delta^{238}\text{U}$ values seems to show a relationship with that of the solid load (Fig. 3b).

The broad positive relationships between dissolved U, Ca, and SO_4 , though with 2–3 outliers (Fig. 2b,c) might be consistent with a lithological control (likely carbonate or black shale weathering) on the dissolved U abundance, as suggested previously (Palmer and Edmond, 1993; Zhou et al., 2015). It is also possible, however, that the correlation with Ca might reflect the fact that U solubility is enhanced through complexation with bicarbonate in well-oxygenated waters such as that of rivers, as also suggested previously (Fig. 2d; Langmuir, 1978; Chabaux et al., 2003; Zhou et al., 2015). A broad positive relationship between dissolved U isotopes and Na^* , again with CAN13–05 as an outlier, could suggest a link with silicate weathering. No relationship emerges between dissolved U isotopes and Ca or SO_4 (Fig. 2f,g), suggesting the absence of a simple lithological control on U isotopes, though water dilution can affect the elemental-isotope comparisons.

The river dissolved U isotope compositions do not show resolvable fractionation with respect to their river solid counterparts (Fig. 3b). This is surprising based on previous work that suggests resolvable U isotope fractionation during weathering processes (Andersen et al., 2016; Noordmann et al., 2016). It also contrasts with what has been observed in other studies in the Mackenzie Basin for which stable isotope ratios are partitioned between the river dissolved and solid loads - the two complementary products - for example light isotope systems such as Li, B and Mg (Lemarchand and Gaillardet, 2006; Millot et al., 2010; Tipper et al., 2012) and heavier isotope systems such as Ba and Re (Dellinger et al., 2021; Charbonnier et al., 2022). Taking the river sediments only, a number of samples display enrichment in heavy U isotopes compared to silicate rocks. This could reflect the preferential scavenging of heavy U isotopes during secondary weathering processes, or a lithological source of heavier U isotope signature than silicates.

The lack of resolvable U isotope differences between the river

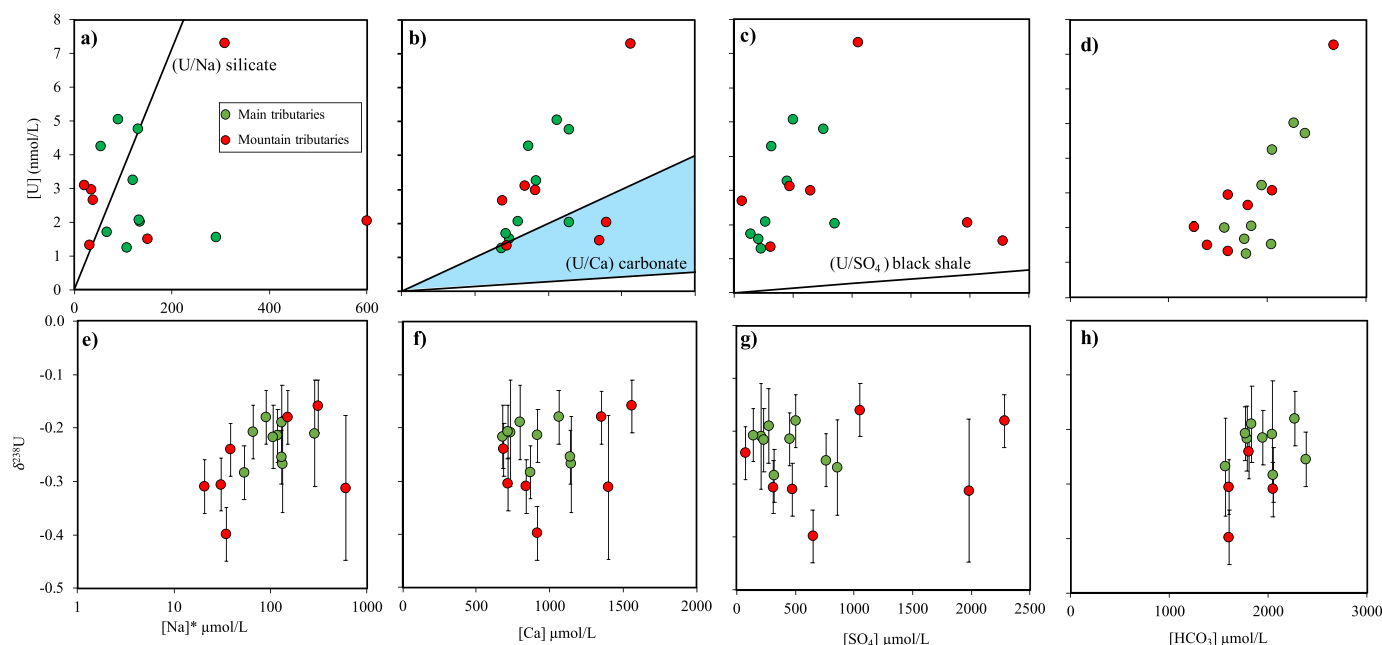


Fig. 2. Scatter plot of dissolved U abundance and isotope composition ($\delta^{238}\text{U}$) vs. sodium derived from silicate weathering (Na^* ; corrected for the sea-salt and evaporite inputs using the measured Cl concentration and the Na/Cl ratio of seawater; Millot et al., 2003), calcium (Ca), sulfate (SO_4) and alkalinity (HCO_3). The U/Na ratio for silicate comes from sedimentary silicate rocks from Taylor and McLennan (1995), the range of U/Ca ratio of carbonate (blue shading) from Clarkson et al. (2021), and the U/ SO_4 for black shale from Kendall et al. (2020). (For interpretation of the references to colour in this figure legend, the reader is referred to the web version of this article.)

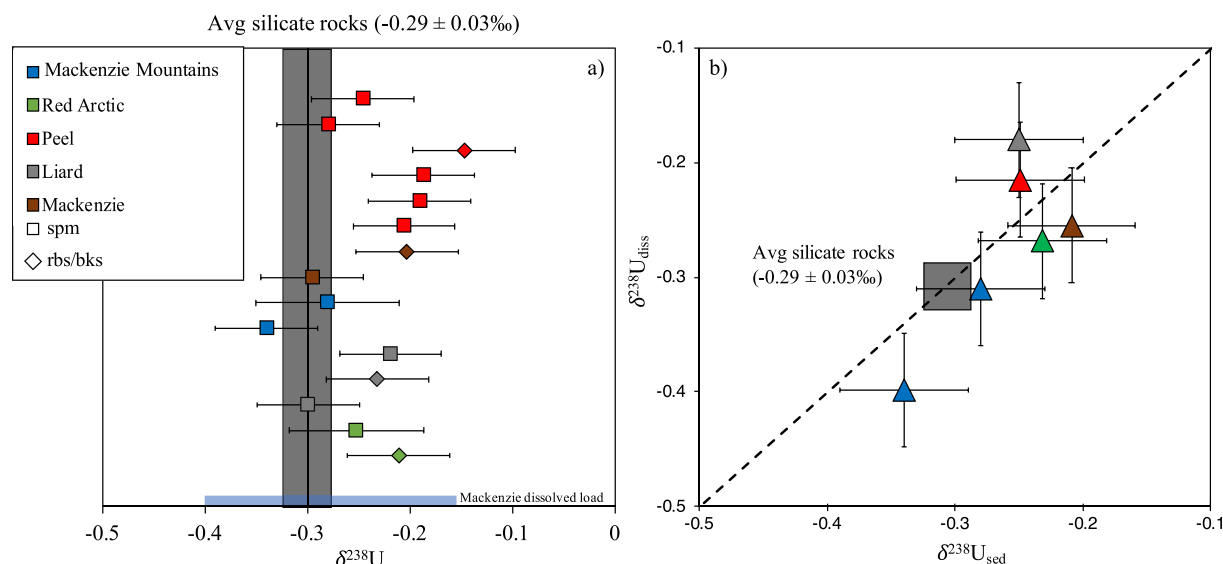


Fig. 3. Uranium isotope composition ($\delta^{238}\text{U}$) in the solid load of the Mackenzie Basin a), and comparison between the $\delta^{238}\text{U}$ of the river dissolved and solid loads of the Mackenzie Basin b). The vertical grey band in (a) and the grey square in (b) represent the U isotope compositions of the average continental crust estimated in Andersen et al. (2015) and Tissot and Dauphas (2015). “spm” corresponds to suspended particulate matter, and “rbs/bks” correspond to river bed sediment and bank material. Where available, the average $\delta^{238}\text{U}$ value of river sediment is shown in b), which does not differ from individual river sediment data.

dissolved and solid loads suggests that U isotopes are not fractionated by weathering processes. Consequently, the low variability in $\delta^{238}\text{U}$ across the Mackenzie Basin tributaries could simply fingerprint the variation in the weighted average $\delta^{238}\text{U}$ of the Mackenzie bedrock captured by rivers. In that regard, the discussion below will first explore the different rock contributions to the weathering and erosion budgets that could drive the variation in both river dissolved and solid $\delta^{238}\text{U}$. Later, we explore the influence of secondary weathering processes on the river dissolved $\delta^{238}\text{U}$.

4.1. Source control on U isotopes in river sediments of the Mackenzie Basin

Because of the overall low weathering intensity (i.e., the relative loss of soluble elements from solids passing through the weathering reactor) in the Mackenzie Basin, river sediments provide a reliable indicator of the source contribution to the physical and chemical weathering budget (Millot et al., 2003; Dellinger et al., 2014; Charbonnier et al., 2022). To account for the dilution caused by U free-phases such as quartz, the U abundance is normalized to that of thorium (Th), an insoluble element having a similar magmatic compatibility (Gaillardet et al., 1999a; Bouchez et al., 2011).

The U/Th ratios of river sediments show a broad positive relationship with $\delta^{238}\text{U}$ in the river sediments studied here (Fig. 4a). The samples with lower U/Th tend towards silicate rock compositions (U/Th \approx 0.25; Ross and Bustin, 2009; Taylor and McLennan, 1995; Rudnick and Gao, 2013), with an inferred silicate $\delta^{238}\text{U}$ end member ($\sim -0.35\text{‰}$) slightly lower than continental crust and detrital silicate phases ($\approx -0.29\text{‰} \pm 0.03$ 2 S.D.; Andersen et al., 2014; Tissot and Dauphas, 2015; Andersen et al., 2016; Clarkson et al., 2021). If this trend is controlled by binary mixing, the samples with U/Th above the silicate rock end member could represent the contribution of a U-enriched source. The two other main rock types in the Mackenzie Basin that could account for this additional U source are black shale and carbonate (Reeder et al., 1972; Millot et al., 2003; Huh et al., 2004; Calmels et al., 2007).

Whilst carbonate is suggested to significantly contribute to river dissolved U (Palmer and Edmond, 1993; Zhou et al., 2015), the new data presented here suggest only a minor role in river sediment because: 1) the Ca/Na ratios of river sediments are low, suggesting that river sediments do not contain appreciable amounts of carbonate; 2) no relationship emerges between Ca/Al and $\delta^{238}\text{U}$ (not shown). The $\delta^{238}\text{U}$ of

carbonates in the Mackenzie Basin is not known, but is expected to be closer to seawater compositions ($-0.38 \pm 0.02\text{‰}$; Kipp et al., 2022) and hence silicate values, though early diagenetic processes could drive it higher (e.g., $+0.27 \pm 0.14\text{‰}$ higher than seawater; Romaniello et al., 2013; Chen et al., 2018). Thus, carbonates have limited potential to drive an increase in $\delta^{238}\text{U}$ with U/Th.

Black shales are known to be highly enriched in U (as reduced U (IV)) and are also typically enriched in ^{238}U (e.g., Ross and Bustin, 2009; Tissot and Dauphas, 2015; Andersen et al., 2017; Clarkson et al., 2023). Consequently, the erosion of black shale could account for the higher U/Th ratios and heavier U isotope signatures found in the river sediments of the Mackenzie Basin. This hypothesis can be further tested using the vanadium (V) to Al ratio of river sediments. Vanadium is relatively insoluble and is also known to be a redox-sensitive element, enriched in black shale (e.g., Tribouillard et al., 2006; Kendall et al., 2020). Hence, the V/Al of river sediments could trace the erosion of black shale, whereas weathering processes should have a minor influence on this ratio (Dellinger et al., 2021). There is also a positive relationship between V/Al and U/Th and $\delta^{238}\text{U}$ (Fig. 4b,c), consistent with mixing between a silicate end member and one with higher V/Al, U/Th and $\delta^{238}\text{U}$, thus also suggesting that black shale erosion contributes to the U isotope budget in the Mackenzie Basin. Furthermore, extrapolation of the V/Al versus $\delta^{238}\text{U}$ trend to the V/Al ratio for black shale from the Mackenzie catchment, inferred in Ross and Bustin (2009), yields a $\delta^{238}\text{U}$ for the eroded black shale in the Mackenzie of around 0‰.

The preservation of a heavy U isotope signature in river sediments from a V- and U-enriched end member, inferred to be black shales, suggests either 1) an erosion rate faster than the U (IV) oxidation rates (as could be the case for the oxidation of petrogenic carbon in the Mackenzie Basin; Hilton et al., 2015; Horan et al., 2019) or 2) U released from black shale weathering is at least partly scavenged by sorption or secondary phase formation. More speculatively, this finding shows that enhanced black shale erosion may have an impact on the $\delta^{238}\text{U}$ of detrital riverine input to the ocean. The authigenic fraction of marine sedimentary archives is typically obtained by correcting bulk compositions for the terrigenous input assuming that the latter exhibits the elemental and isotope compositions of silicate (e.g., Tribouillard et al., 2006; Clarkson et al., 2021). As a result, an increase in black shale erosion could lead to an overestimation of the reducing condition recorded in such sedimentary archives.

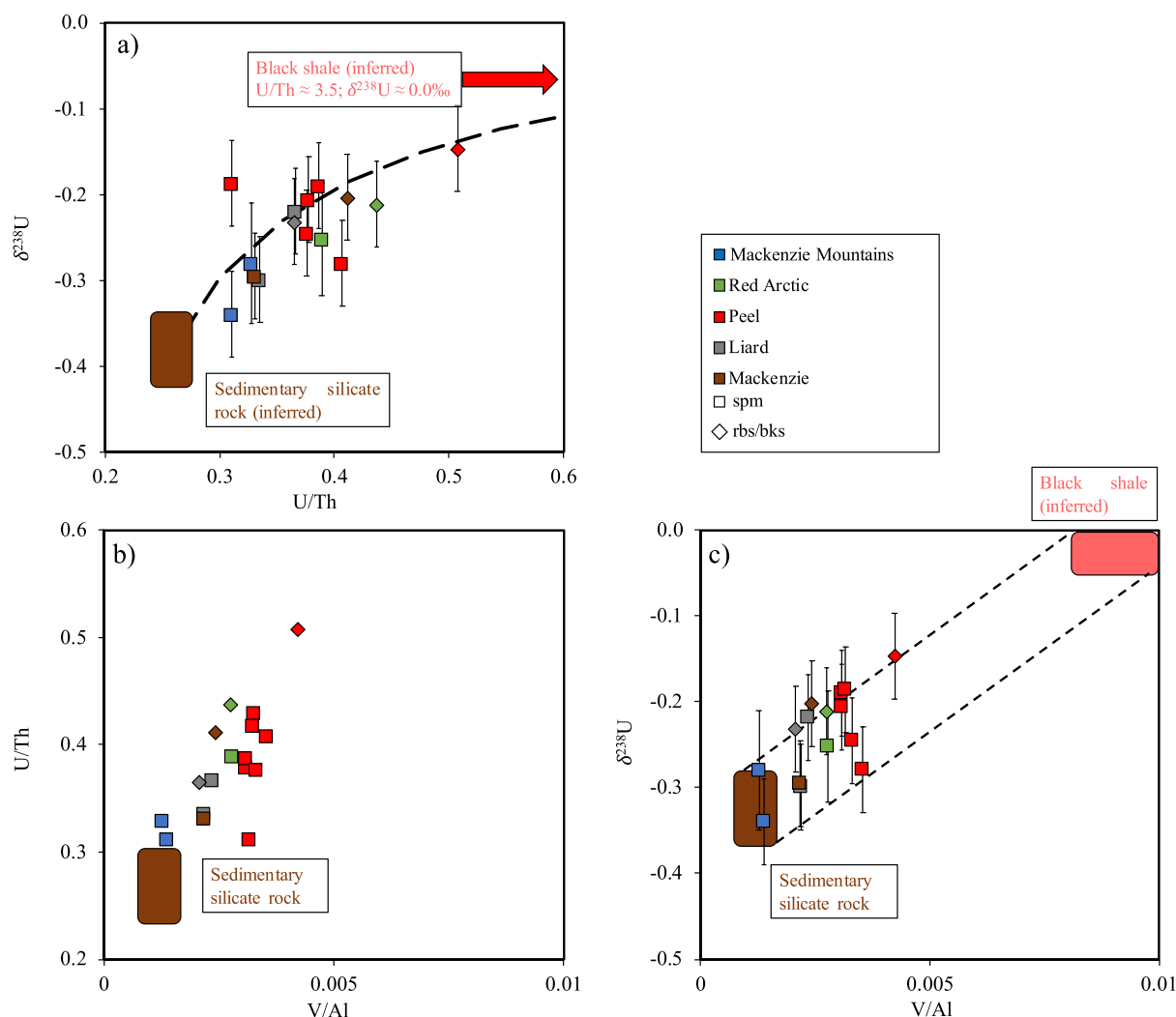


Fig. 4. Uranium isotope composition ($\delta^{238}\text{U}$) vs a) U/Th ratio, b) U/Th vs. V/Al, and c) $\delta^{238}\text{U}$ vs. V/Al ratio for river sediments from the Mackenzie Basin. The U/Th and V/Al ratios of the sedimentary silicate end member come from Taylor and McLennan (1995) and Rudnick and Gao (2013). The V/Al and U/Th ratios of black shale from the Mackenzie Basin come from Ross and Bustin (2009) and is compiled in Dellinger et al. (2021). The $\delta^{238}\text{U}$ of the sedimentary silicate rock and black shale end members on these diagrams is defined by extrapolation of the trends to the V/Al and U/Th values of silicate rocks.

4.2. Testing the source control on U isotope composition of the dissolved load

4.2.1. Assessing the source of U in the Mackenzie Basin

Overall, the different relationships between dissolved U, U isotopes and major elements are challenging to interpret, and might suggest multiple sources contributing to the dissolved U budget. The assessment of the different source contributions to the solutes of the Mackenzie Basin tributaries allows their influence on the dissolved elemental U budget to be explored. First, it is unlikely that sea-salt input influences the dissolved U budget across the Mackenzie Basin tributaries. Even if all of the Cl derives from sea salt input, and using the U/Cl of the seawater of around 2×10^{-5} nmol/ μmol , U deriving from sea salt cannot account for $>0.1\%$ of the total dissolved U budget. Based on a positive relationship between Na, Cl and U, halite has been suggested to contribute to the dissolved U budget of rivers (Zhou et al., 2015). However, no relationship is observed between dissolved U, Na and Cl (not shown). Again, even assuming that all the Cl derives from halite dissolution, the U/Cl ratio of halite provided in Tissot and Dauphas (2015) is too low to represent a substantial source of dissolved U, as for sea salt input. Similarly, gypsum dissolution should not influence the dissolved U inventory. The low U/SO₄ ratio of gypsum associated with the low

contribution of gypsum to the river SO₄ budget across the Mackenzie Basin tributaries again makes gypsum dissolution an unlikely source of U (Tissot and Dauphas, 2015).

The data in Fig. 2c show large U excesses relative to SO₄ compared to a first-order estimate of the U/SO₄ ratio of black shale from the Mackenzie Basin (roughly 1–3% of S and 40 ppm of U; Kendall et al., 2020). Only two rivers, CAN13–05 and CAN13–14, clear outliers on Fig. 2c, exhibit U/SO₄ ratio relatively close to this ratio. Carbonate weathering has also been cited as a potential source of dissolved U (Palmer and Edmond, 1993; Zhou et al., 2015). However, the Mackenzie samples again show an excess of U over Ca relative to the range of U/Ca ratios for carbonate represented by the blue shaded field in Fig. 2b (Palmer and Edmond, 1993; Zhou et al., 2015; Clarkson et al., 2021). The positive relationship between U and Ca may in fact be simply a result of the positive relationship between U and HCO₃, reflecting the relationship between U solubility and carbonate ligands (Langmuir, 1978; Palmer and Edmond, 1993; Chabaux et al., 2003). Silicate weathering has never been considered as a significant source of dissolved U (Palmer and Edmond, 1993; Zhou et al., 2015). However, the U/Na ratio of silicate sedimentary rocks (that represent the main silicate rock type in the Mackenzie Basin) reported in the U–Na* diagram (Fig. 2a) suggests that silicate weathering could, for most rivers, supply more dissolved U than

observed in the Mackenzie Basin.

Overall, this comparison between dissolved U and major elements suggests that the weathering of multiple rock types might contribute to the riverine U budget. But deconvolving the quantitative contribution of each of these sources is challenging using single elemental abundances. Further, the lack of significant input from black shale might appear surprising given other evidence reported in the literature (e.g., Reeder et al., 1972; Palmer and Edmond, 1993), and given the relatively clear contribution to the particulate load (Fig. 4). One potential explanation for this discrepancy could be variability in the black shale U/SO₄ ratio, since uranium and sulfur are hosted in different mineral phases within black shale. In the following section, we use the isotope signatures of U in the river dissolved and solid loads of the Mackenzie to investigate the relative role of sources in setting the dissolved U elemental and isotope river fluxes.

4.2.2. Lithological controls on dissolved U isotopes

The river sediments provide the first indications of a silicate rock (and black shale) control on the U isotope riverine budget (Fig. 4). Moreover, the 1:1 relationship between $\delta^{238}\text{U}$ of the river dissolved and solid loads could suggest a source control on the river dissolved $\delta^{238}\text{U}$

(Fig. 3b), in particular from silicate and black shale (see section 4.1). This, added to the fact that elemental compositions suggest that various sources could, in principle, influence the dissolved U inventory (section 4.2.1), leads us to first examine the potential for a source control on the U isotopes of the dissolved load.

Previous studies on dissolved U abundances argued in favour of the potential control of carbonate and black shale weathering on the dissolved U budget (e.g., Palmer and Edmond, 1993; Dunk et al., 2002; Zhou et al., 2015). The broad positive relationship observed between dissolved U, Ca, and SO₄ as well as the positive correlation of $\delta^{238}\text{U}$, U/Th and V/Al in river sediments (sections 4.1 and 4.2.1) further argue in favour of this lithological control. These different rock types are known to have distinct U isotope signatures (Weyer et al., 2008; Romaniello et al., 2013; Tissot and Dauphas, 2015), which could, in turn, explain the variations in the dissolved $\delta^{238}\text{U}$ across the Mackenzie Basin. For this reason, carbonate and black shale weathering controls are first examined.

Carbonates tend to have relatively low U concentrations (e.g., Romaniello et al., 2013; Clarkson et al., 2020) but have been proposed as a substantial U source at the catchment scale (Palmer and Edmond, 1993; Zhou et al., 2015). Further, the strong influence of carbonate

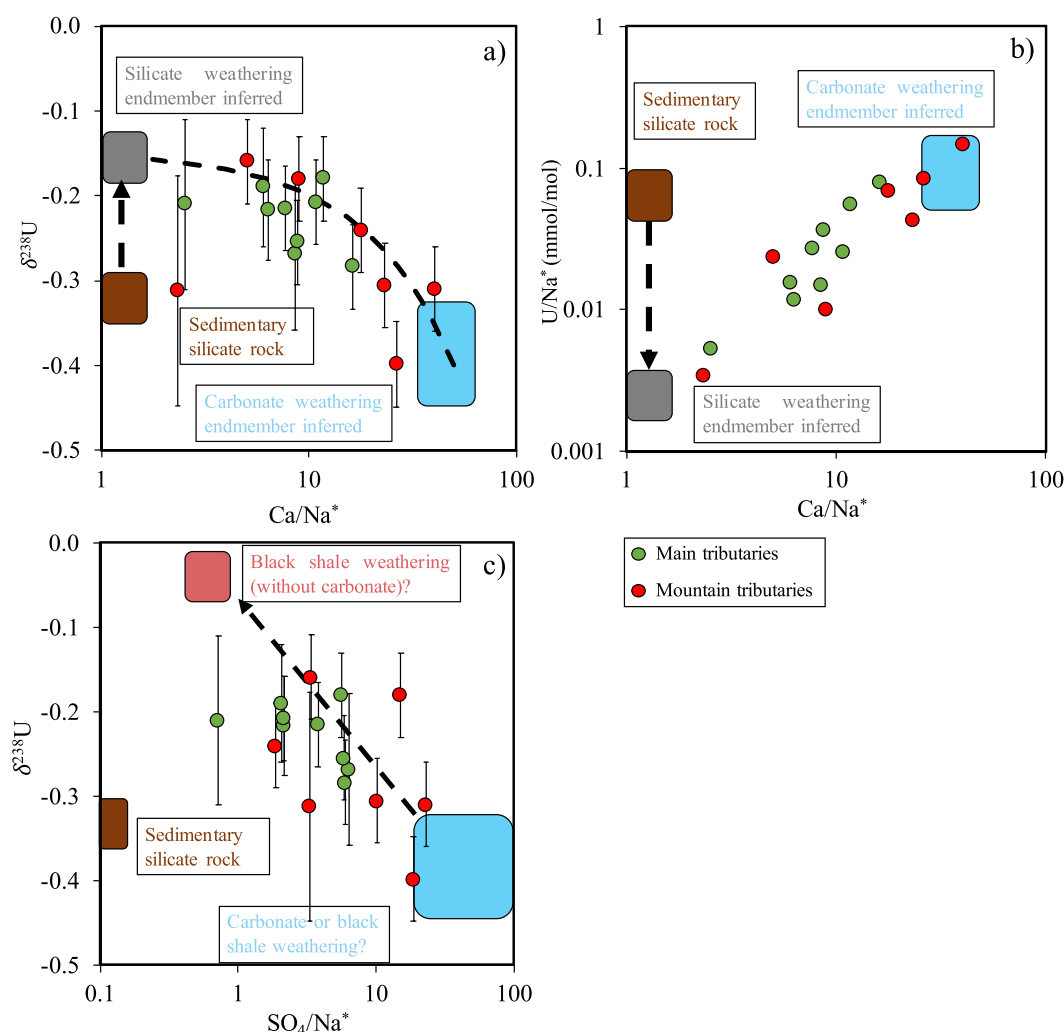


Fig. 5. Scatter plot of dissolved Ca/Na* vs. $\delta^{238}\text{U}$ a) and U/Na* b); and SO₄/Na* vs. $\delta^{238}\text{U}$ c) ("*" corresponds to the correction for sea salt and halite inputs; Millot et al., 2003). The dissolved Ca/Na*, SO₄/Na* and the Ca/Na of silicate (grey) and carbonate (blue) end-members come from Millot et al. (2003). The $\delta^{238}\text{U}$ of the carbonate end-member is inferred from the interpretation of the data arrays in terms of mixing. The brown box in panels a and b indicates the probable position of sedimentary silicate rocks, which is similar in term of $\delta^{238}\text{U}$ to the continental crust estimated in Tissot and Dauphas (2015). The vertical dashed arrows in panels a and b indicate how the end-members inferred from the data array differ from this probable sedimentary silicate end-member. (For interpretation of the references to colour in this figure legend, the reader is referred to the web version of this article.)

weathering (in comparison to silicate weathering; Millot et al., 2003) in the Mackenzie Basin has been noted previously. Here, the carbonate weathering influence on dissolved U isotopes is examined by plotting both dissolved $\delta^{238}\text{U}$ and U/Na^* against the dissolved Ca/Na^* (used here as a tracer of the silicate vs. carbonate contributions; Fig. 5a,b; Gailardet et al., 1999b). As noted earlier, the evidence from elemental relationships is mixed in terms of a significant contribution from black shale, but we also test the possibility of this influence on dissolved $\delta^{238}\text{U}$ by examining the data as a function of SO_4/Na^* (where SO_4 is corrected for gypsum contribution when it is possible; Fig. 5c; Calmels et al., 2007). Higher SO_4/Na^* ratios indicate a greater influence of black shale weathering, whereas lower SO_4/Na^* ratios indicate a lesser influence.

Dissolved $\delta^{238}\text{U}$ is negatively correlated, and U/Na^* positively correlated, with Ca/Na^* (Fig. 5a,b). In theory, these elemental ratio relationships are compatible with binary mixing between 1) average silicate, (low Ca/Na^* and lower U/Na^*) and 2) carbonate (high Ca/Na^*). However, the end members inferred with these elemental relationships do not match with those expected for the U isotope compositions.

The first end member, the low U/Na^* , Ca/Na^* and SO_4/Na^* end member, that should reflect the silicate weathering end member, exhibits an extrapolated $\delta^{238}\text{U}$ of $\sim -0.15\text{‰}$, which is not consistent with average silicate rocks (-0.29‰ ; Tissot and Dauphas, 2015). The $\delta^{238}\text{U}$ value for the silicate end member inferred from the river sediments (using the relationship between U/Th and $\delta^{238}\text{U}$; Fig. 4a in section 4.1) indicates a $\delta^{238}\text{U}$ for silicates only slightly lighter (-0.35‰) than that for average silicate rocks. In addition, the dissolved U/Na^* of the silicate weathering end member obtained by extrapolation of the dissolved $\text{U}/\text{Na}^*-\text{Ca}/\text{Na}^*$ trend is two orders of magnitude lower than that of sedimentary silicate rocks (Fig. 5b; Taylor and McLennan, 1995; Rudnick and Gao, 2013).

The second end member, exhibiting high U/Na^* , Ca/Na^* and SO_4/Na^* , converges towards a low $\delta^{238}\text{U}$ of around (-0.40‰). For this end member, elemental ratios are consistent with the weathering of carbonate. The low $\delta^{238}\text{U}$ is not consistent with a black shale end member. Though similar light values have been reported for some black shales (Kendall et al., 2020), the $\delta^{238}\text{U}$ of black shale inferred with river sediments suggests an overall higher value (around 0‰ ; see section 4.1). Thus, the $\delta^{238}\text{U}$ value for this end member only matches that of a carbonate (Romaniello et al., 2013; Andersen et al., 2017; Clarkson et al., 2020). But it also seems unlikely that, in a context of both strong carbonate and black shale weathering, U release from carbonate weathering can overprint the one from black shale weathering, as U is much more enriched in black shale than in carbonate (Romaniello et al., 2013; Clarkson et al., 2020; Kendall et al., 2020).

Taken together, the relationships observed between $\delta^{238}\text{U}$, U/Na^* , SO_4/Na^* and Ca/Na^* suggest mixing between two end-members. But the $\delta^{238}\text{U}$ values for the end members inferred from the mixing relationships are not consistent with either the literature or the end members deduced from the $\delta^{238}\text{U}$ of river sediments. In other words, while the $\delta^{238}\text{U}$ of river sediments shows a binary mixing between silicate minerals and black shales, the $\delta^{238}\text{U}$ of the river dissolved load does not reflect the same mixing pattern. This finding is intriguing since the positive relationship between river dissolved and solid $\delta^{238}\text{U}$ should indicate a source control on the river dissolved load (Fig. 3b). We are left with a conundrum concerning the relationship between the riverine $\delta^{238}\text{U}$ dissolved and solid loads that is challenging to solve given the current state of knowledge on U isotopes in rivers (see review of Andersen et al., 2017).

An alternative way to explore the dissolved $\delta^{238}\text{U}$ is to leave aside the relationship between $\delta^{238}\text{U}$ of the river dissolved and solid loads, and consider the dissolved $\delta^{238}\text{U}$ on its own. In this respect, we note that silicate weathering could be the dominant source of dissolved U across the Mackenzie Basin tributaries. Furthermore, silicate weathering theoretically supplies more dissolved U than found in rivers (see section 4.2.1 and Fig. 2a), suggesting that a significant amount of the U released

from silicate dissolution is scavenged through secondary weathering processes. We explore this hypothesis below.

4.3. Testing the control of weathering processes on the U isotope composition of the dissolved load

4.3.1. Quantifying the extent of U scavenging through secondary weathering processes

The discussion in the last section points to the need for controls on the dissolved U abundance and isotope composition over and above source lithology. Sodium is widely used as a normalising element in studies of chemical weathering due to its conservative behaviour (e.g., Gislason et al., 1996). As noted in the previous section (Fig. 5b), the dissolved U/Na^* ratio shows a clear positive correlation with Ca/Na^* . But this correlation requires an end member with a U/Na ratio that is two orders of magnitude below carbonate or sedimentary silicate (Taylor and McLennan, 1995; Ross and Bustin, 2009; Romaniello et al., 2013; Rudnick and Gao, 2013; Andersen et al., 2017), and thus loss of U from the dissolved phase relative to Na. Although reduction to immobile U (IV) (Stirling et al., 2007; Weyer et al., 2008; Andersen et al., 2017) is one of such potential loss process, this seems unlikely in the oxidising weathering environment. Sorption onto surfaces (Jemison et al., 2016), and/or incorporation into secondary phases formed during weathering (Brennecke et al., 2011b; Ma et al., 2012; Holmden et al., 2015) seem more likely. Oxidative dissolution of reduced U phases is thought not to involve U isotope fractionation (Wang et al., 2015; Clarkson et al., 2021).

Lower dissolved U/Na^* appears to be generally associated with higher $\delta^{238}\text{U}$ (Fig. 6a), suggesting that the depletion of uranium in the dissolved load (low U/Na^*) could be associated with heavier dissolved $\delta^{238}\text{U}$ signatures (by around -0.20‰), consistent with preferential adsorption of ^{235}U onto secondary mineral phases (Brennecke et al., 2011b; Jemison et al., 2016). The data array appears to converge towards the U/Na ratio of grey shale from the Mackenzie reported in Ross and Bustin (2009) and a $\delta^{238}\text{U}$ close to that of silicates. As an additional constraint, the silicate end member indicated by the dissolved $\text{U}/\text{Na}^*-\delta^{238}\text{U}$ trend is also consistent, for both U/Na and $\delta^{238}\text{U}$, with the silicate end member inferred with river sediments (section 4.1; Table 2), and thus not far from igneous or clastic sedimentary rocks.

Following Bouchez et al. (2013), the relationship between the fraction of U taken up by secondary processes and U isotope composition can be described as follows:

$$\delta^{238}\text{U}_{\text{diss}} = \delta^{238}\text{U}_{\text{rock}} - \Delta_{i-\text{diss}} \times (1 - f_{\text{diss}}^{\text{U}}) \quad (3)$$

where $\delta^{238}\text{U}_{\text{diss}}$, $\delta^{238}\text{U}_{\text{rock}}$, are the isotope composition of the river dissolved load and the bedrock estimated using the data array in Fig. 6a; $\Delta_{i-\text{diss}}$ is the isotope fractionation by process i ; $f_{\text{diss}}^{\text{U}}$ is the fraction of U remaining in solution after uptake by secondary processes:

$$f_{\text{diss}}^{\text{U}} = \frac{\left(\frac{\text{U}}{\text{Na}}\right)_{\text{diss}}^*}{\left(\frac{\text{U}}{\text{Na}}\right)_{\text{rock}}} \quad (4)$$

where $\left(\frac{\text{U}}{\text{Na}}\right)_{\text{diss}}^*$ is the uranium over sodium ratio of the river dissolved load (corrected for sea salt and evaporite inputs) and $\left(\frac{\text{U}}{\text{Na}}\right)_{\text{rock}}$ the uranium over sodium ratio of the average rock undergoing weathering – using the grey shale from the Mackenzie Basin (Ross and Bustin, 2009).

The negative relationship observed between the dissolved U/Na^* and $\delta^{238}\text{U}$ suggests that secondary minerals take up the light U isotope (negative $\Delta_{i-\text{diss}}$ in eq. 3). This confirms that formation of reduced U phases after silicate rock dissolution is not a relevant process here, as this preferentially take up heavy isotopes (Stirling et al., 2007; Weyer et al., 2008). The best fit is found for a fractionation factor around -0.1 to -0.2‰ (Fig. 6b). This fractionation factor is compatible with the

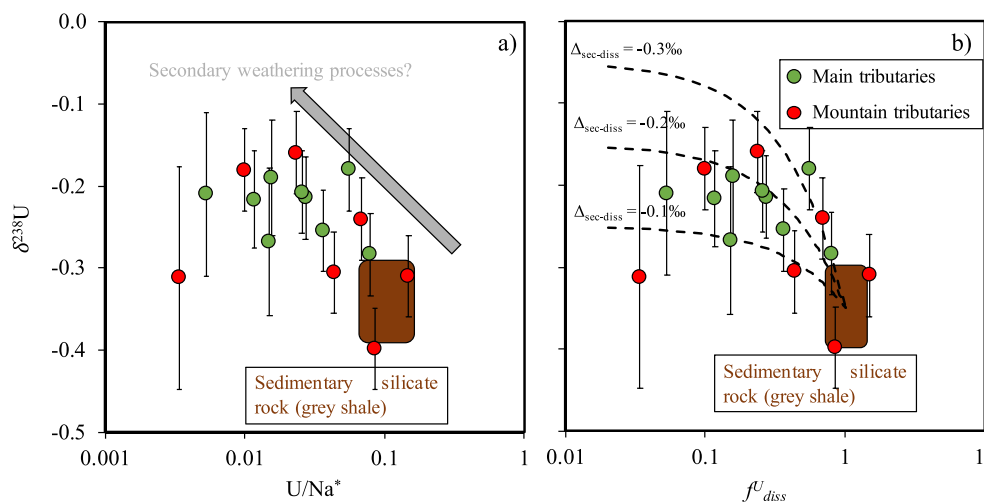


Fig. 6. The dissolved $\delta^{238}\text{U}$ vs. a) the dissolved U/Na^* ratio and b) the fraction of U remaining after rock dissolution (see eq. 4). The model curves in b represent theoretical isotope fractionation during weathering processes in an open-flow-through system described with eq. 3, for various values of $\Delta_{\text{sec-diss}} = \delta^{238}\text{U}$ for a secondary mineral formed in the weathering environment minus $\delta^{238}\text{U}$ for the dissolved phase. The brown box corresponds to the estimate U/Na and $\delta^{238}\text{U}$ of sedimentary silicate rocks. The silicate sedimentary rocks are estimated from Ross and Bustin (2009) for the U/Na ratio and $\delta^{238}\text{U}$ from the silicate endmember inferred with the river sediments and the literature (see section 4.1; Tissot and Daplas, 2015). (For interpretation of the references to colour in this figure legend, the reader is referred to the web version of this article.)

average values for sorption onto residual mineral phases ($\Delta_{\text{sorp-diss}} = -0.20\text{‰}$; Brennecka et al., 2011b; Jemison et al., 2016). Besides sorption, light uranium is thought to be preferentially incorporated into secondary minerals (Holmden et al., 2015), although isotope fractionation for $\delta^{238}\text{U}$ is not well constrained. Whatever the precise process, our findings provide a first estimation of the fractionation factor for processes that preferentially retain U in residual solids in the weathering environment, at basin-scale.

4.3.2. Controlling factors of the extent of U scavenging processes

If secondary phase formation is a driver of the river dissolved $\delta^{238}\text{U}$ - again considering that the relationship between the river dissolved and solid $\delta^{238}\text{U}$ is somehow co-incidental - the extent of secondary phase formation may reflect the weathering regime and climate (e.g., Lemarchand and Gaillardet, 2006; Millot et al., 2010; Dellinger et al., 2015). These controlling factors are investigated below.

The residence time of solid and fluid in the weathering reactor is known to exert a strong control on chemical reactions, by influencing the partitioning of an element and its isotopes between the dissolved and solid phases (e.g., Ferrier and Kirchner, 2008; Maher, 2010; Bouchez et al., 2013). Solid residence time can be quantified using the weathering intensity (Bouchez et al., 2014), indexed as the ratio between the specific silicate weathering (W) and the total denudation fluxes (D), where increase in W/D is representative of longer solid residence time in the weathering environment. These fluxes are quantified using the silicate weathering-derived cation concentrations (Na, K, Mg, Ca and Si), which are converted into $\text{t/km}^2/\text{yr}$ using the river water discharge and the size of each catchment for the silicate weathering flux W (Gaillardet et al., 1999b). The parameter D is quantified using the sum of the long-term erosion flux (concentration of river suspended particulate matter, which is also converted into $\text{t/km}^2/\text{yr}$ using river water discharge and size of the catchment) and W flux (Carson et al., 1998; Millot et al., 2003; Bouchez et al., 2014; Dellinger et al., 2015). Fluid residence time also regulates silicate weathering reactions and isotope partitioning (Johnson et al., 1997; Maher, 2011), exerting a strong control on the sorption of boron onto particles in soils of the Mackenzie lowland (Lemarchand and Gaillardet, 2006). Runoff may be used to estimate the amount of time water spends in the weathering reactor. Low runoff is associated with longer interaction between water and the mineral surfaces, while high runoff makes the water-rock interactions shorter. Therefore, the comparison between U, its isotopes and W/D and runoff offers another perspective on the weathering reaction control on U.

The $\delta^{238}\text{U}$ shows a broad positive relationship with W/D and runoff, whilst U/Na^* shows a broad negative relationship (Figs. 7). Collectively, these results might support the process control hypothesis on the river

dissolved U and $\delta^{238}\text{U}$. On the one hand, the relationships between dissolved U/Na^* and $\delta^{238}\text{U}$ and W/D are consistent with the suggestion that the extent of U scavenging is driven by the solid residence time — as it is the case for Li (Millot et al., 2010; Dellinger et al., 2015). Indeed, when the residence time is short (low W/D), the solids are rapidly exported from the weathering reactors, thus hampering the formation of secondary phases such as clays or oxy-hydroxides after primary rock dissolution (Bouchez et al., 2013). Thus, $\delta^{238}\text{U}$ and U/Na^* are close to the average estimate of the Mackenzie bedrock in this fast eroding setting. When the residence time is longer (high W/D), the formation of secondary phase is enabled, leading to uptake of the dissolved U (compared to Na) and its light isotopes. On the other hand, the relationship between dissolved U/Na^* , $\delta^{238}\text{U}$ and runoff might suggest that longer water-rock interaction may increase the scavenging of U (compared to Na) and its light isotopes. When the water residence time is shorter (high runoff), uranium released from rock weathering is rapidly exported from the weathering reactor, thus inhibiting the exchange between U and mineral surfaces, yielding U/Na^* and $\delta^{238}\text{U}$ close to the source rocks. These relationships between dissolved U, its isotopes and runoff are consistent with the observations made for boron and its isotopes in the Mackenzie (Lemarchand and Gaillardet, 2006).

Overall, the trends between dissolved $\delta^{238}\text{U}$, weathering regime and runoff support the hypothesis of a control on $\delta^{238}\text{U}$ in the Mackenzie Basin through secondary processes in the weathering environment. However, determining which of solid or fluid residence times control the partitioning of U between the dissolved and solid phases remains a challenge.

5. Conclusion and implications

In this study, we report a comprehensive dataset of $\delta^{238}\text{U}$ and U concentrations in both river dissolved and solid loads in the Mackenzie Basin. The dissolved $\delta^{238}\text{U}$ ranges from -0.15 to -0.39‰ , while the range in the isotope composition of river sediments (-0.14 to -0.34‰) is the same as the dissolved load. Furthermore, the dissolved $\delta^{238}\text{U}$ are well related to their $\delta^{238}\text{U}$ river sediment counterpart. Overall, both U in the river dissolved and solid loads display subtle but resolvable isotope differences with respect to the continental crust, that can be attributed to source mixing and secondary processes.

Uranium in the river solid load seems to be driven by mixing between two sources represented by 1) the erosion of silicate (U/Th and $\delta^{238}\text{U}$ relatively similar to average silicate rocks) and 2) the erosion of U deriving from black shale (higher U/Th and $\delta^{238}\text{U}$ than average silicate rocks).

The $\delta^{238}\text{U}$ of the river dissolved load shows some apparent binary mixing between carbonate and possibly black shale. Nonetheless,

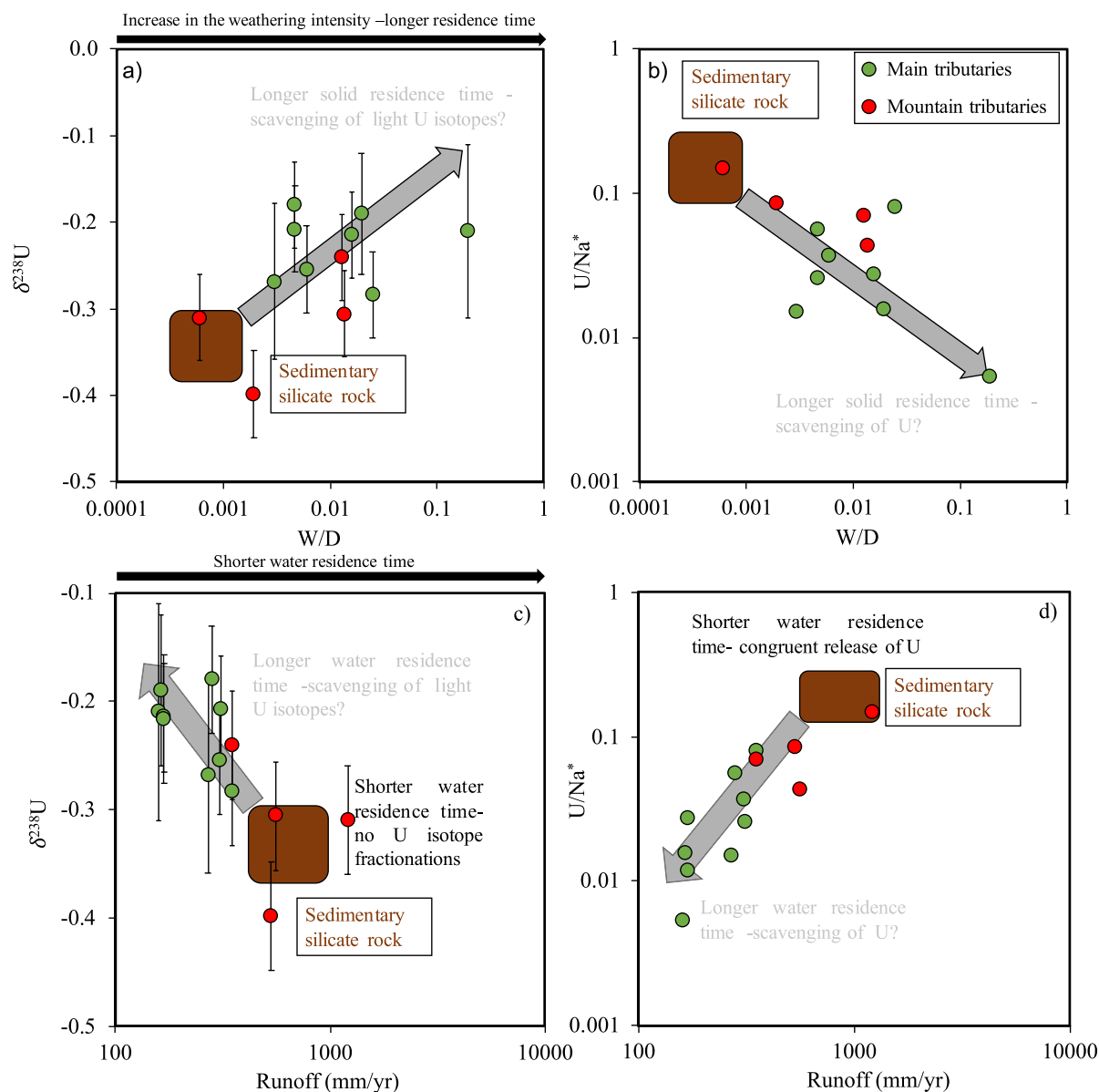


Fig. 7. Dissolved $\delta^{238}\text{U}$ a) and U/Na^* b) vs. the weathering intensity, as estimated from the ratio of the silicate weathering flux over the denudation flux (W/D). Data on W/D comes from [Dellinger et al. \(2015\)](#), and $\delta^{238}\text{U}$ c) and U/Na^* d) vs. runoff. Runoff data come from [Millot et al. \(2003\)](#). The brown box corresponds to the estimate U/Na and $\delta^{238}\text{U}$ of sedimentary silicate rocks. The silicate sedimentary rocks are estimated from [Ross and Bustin \(2009\)](#) for the U/Na ratio and $\delta^{238}\text{U}$ from the silicate endmember inferred with the literature (see [section 4.1](#); [Tissot and Dauphas, 2015](#)). (For interpretation of the references to colour in this figure legend, the reader is referred to the web version of this article.)

inconsistencies in SO_4/Na^* , U/Na^* and Ca/Na^* characteristics make this explanation unlikely. This finding is particularly intriguing since the river dissolved $\delta^{238}\text{U}$ do not show isotope differences with their river sediment, suggesting an initial source control on the dissolved $\delta^{238}\text{U}$. Fractionation of U isotopes by the secondary processes following silicate weathering could alternatively explain the data, but implies a limited influence of source controls on the U dissolved budget. The broad positive relationships between the dissolved U/Na^* , $\delta^{238}\text{U}$, runoff and the weathering intensity might suggest a residence time control on the reactions that scavenge the dissolved U into secondary phase or sorption onto particles. Indeed, longer residence times of water and solid allow for a more intense scavenging of U following rock weathering. By contrast, shorter residence time of water hampers the uptake of the dissolved U by secondary phase or sorption onto particles.

Overall, our study highlights both source and weathering processes as dual controlling factors on the river dissolved $\delta^{238}\text{U}$. Further work is

required to determine whether or not the positive correlation between dissolved and solid $\delta^{238}\text{U}$ truly reflects a source control on the river dissolved $\delta^{238}\text{U}$ or is simply co-incidental. In the case of a co-incidental relationship, this might suggest that secondary weathering processes are able to fractionate U isotopes, driving the riverine $\delta^{238}\text{U}$ towards higher values depending on the weathering regime on geological timescales ([Misra and Froelich, 2012](#)), adding further complications to understanding ancient $\delta^{238}\text{U}$ records.

Authors contribution

Charbonnier: Designed the study, performed new analytical work, interpreted the data, draft preparation. **Hilton:** interpreted the data, draft preparation. **Clarkson:** Assisted with analysis, interpretation and writing. **Vance:** Designed the study, interpreted the data, draft preparation.

Declaration of Competing Interest

The authors declare that they have no known competing financial interests or personal relationships that could have appeared to influence the work reported in this paper.

Data availability

The authors are unable or have chosen not to specify which data has been used.

Acknowledgement

The authors thank Corey Archer for analytical support. This research was supported by Swiss National Science Foundation grant 200021-184873 to DV. Christian France-Lanord is thanked for his efficient editorial handling of the paper. François Tissot and an anonymous reviewer are thanked for their constructive comments. Julien Bouchez and Jérôme Gaillardet are thanked for sharing their samples.

Appendix A. Supplementary data

Supplementary data to this article can be found online at <https://doi.org/10.1016/j.chemgeo.2023.121409>.

References

- Andersen, M.B., Romaniello, S., Vance, D., Little, S.H., Herdman, R., Lyons, T.W., 2014. A modern framework for the interpretation of $^{238}\text{U}/^{235}\text{U}$ in studies of ancient ocean redox. *Earth Planet. Sci. Lett.* 400, 184–194. Available at: <https://doi.org/10.1016/j.epsl.2014.05.051>.
- Andersen, M.B., Elliott, T., Freymuth, H., Sims, K.W.W., Niu, Y., Kelley, K.A., 2015. The terrestrial uranium isotope cycle. *Nature* 517, 356–359. Available at: <https://doi.org/10.1038/nature14062>.
- Andersen, M.B., Vance, D., Morford, J.L., Bura-Nakić, E., Breitenbach, S.F.M.M., Och, L., 2016. Closing in on the marine $^{238}\text{U}/^{235}\text{U}$ budget. *Chem. Geol.* 420, 11–22.
- Andersen, M.B., Stirling, C.H., Weyer, S., 2017. Uranium isotope fractionation. *Non-Trad. Stable Isot.* 82, 799–850.
- Asael, D., Tissot, F.L.H., Reinhard, C.T., Rouxel, O., Dauphas, N., Lyons, T.W., Ponzevara, E., Liorzou, C., Chéron, S., 2013. Coupled molybdenum, iron and uranium stable isotopes as oceanic paleoredox proxies during the Paleoproterozoic Shunga Event. *Chem. Geol.* 362, 193–210. Available at: <https://doi.org/10.1016/j.chemgeo.2013.08.003>.
- Bouchez, J., Gaillardet, J., France-Lanord, C., Maurice, L., Dutra-Maia, P., 2011. Grain size control of river suspended sediment geochemistry: Clues from Amazon River depth profiles. *Geochim. Geophys. Geosyst.* 12.
- Bouchez, J., Von Blanckenburg, F., Schuessler, J.A., 2013. Modeling novel stable isotope ratios in the weathering zone. *Am. J. Sci.* 313, 267–308.
- Bouchez, J., Gaillardet, J., von Blanckenburg, F., 2014. Weathering intensity in lowland river basins: from the Andes to the Amazon mouth. *Proc. Earth Planet. Sci.* 10, 280–286.
- Brenneka, G.A., Herrmann, A.D., Algeo, T.J., Anbar, A.D., 2011a. Rapid expansion of oceanic anoxia immediately before the end-Permian mass extinction. *Proc. Natl. Acad. Sci. U. S. A.* 108, 17631–17634.
- Brenneka, G.A., Wasylenski, L.E., Bargar, J.R., Weyer, S., Anbar, A.D., 2011b. Uranium isotope fractionation during adsorption to Mn-oxhydroxides. *Environ. Sci. Technol.* 45, 1370–1375.
- Brown, S.T., Basu, A., Ding, X., Christensen, J.N., DePaolo, D.J., 2018. Uranium isotope fractionation by abiotic reductive precipitation. *Proc. Natl. Acad. Sci. U. S. A.* 115, 8688–8693.
- Bura-Nakić, E., Andersen, M.B., Archer, C., de Souza, G.F., Marguš, M., Vance, D., 2018. Coupled Mo-U abundances and isotopes in a small marine euxinic basin: Constraints on processes in euxinic basins. *Geochim. Cosmochim. Acta* 222, 212–229.
- Calmels, D., Gaillardet, J., Brenot, A., France-Lanord, C., 2007. Sustained sulfide oxidation by physical erosion processes in the Mackenzie River basin: climatic perspectives. *Geology* 35, 1003–1006.
- Carson, M.A., Jasper, J.N., Conly, F.M., 1998. Magnitude and sources of sediment input to the Mackenzie Delta, Northwest Territories, 1974–94. *Arctic* 116–124.
- Chabaux, F., Riotte, J., Dequincey, O., 2003. U-Th-Ra Fractionation during Weathering and River Transport.
- Charbonnier, Q., Bouchez, J., Gaillardet, J., Calmels, D., Dellinger, M., 2022. The influence of black shale weathering on riverine barium isotopes. *Chem. Geol.* 594, 120741.
- Chen, X., Romaniello, S.J., Herrmann, A.D., Hardisty, D., Gill, B.C., Anbar, A.D., 2018. Diagenetic effects on uranium isotope fractionation in carbonate sediments from the Bahamas. *Geochim. Cosmochim. Acta* 237, 294–311. Available at: <https://doi.org/10.1016/j.gca.2018.06.026>.
- Clarkson, M.O., Stirling, C.H., Jenkyns, H.C., Dickson, A.J., Porcelli, D., Moy, C.M., Von Strandmann, P.P.A.E., Cooke, I.R., Lenton, T.M., 2018. Uranium isotope evidence for two episodes of deoxygenation during Oceanic Anoxic Event 2. *Proc. Natl. Acad. Sci. U. S. A.* 115, 2918–2923.
- Clarkson, M.O., Müsing, K., Andersen, M.B., Vance, D., 2020. Examining pelagic carbonate-rich sediments as an archive for authigenic uranium and molybdenum isotopes using reductive cleaning and leaching experiments. *Chem. Geol.* 539, 119412. Available at: <https://doi.org/10.1016/j.chemgeo.2019.119412>.
- Clarkson, M.O., Hennekam, R., Sweere, T.C., Andersen, M.B., Reichart, G.J., Vance, D., 2021. Carbonate associated uranium isotopes as a novel local redox indicator in oxidatively disturbed reducing sediments. *Geochim. Cosmochim. Acta* 311, 12–28. Available at: <https://doi.org/10.1016/j.gca.2021.07.025>.
- Clarkson, M.O., Sweere, T.C., Chiu, C.F., Hennekam, R., Bowyer, F., Wood, R.A., 2023. Environmental controls on very high $\delta^{238}\text{U}$ values in reducing sediments: implications for Neoproterozoic seawater records. *Earth-Sci. Rev.* 237, 104306. Available at: <https://doi.org/10.1016/j.earscirev.2022.104306>.
- Dahl, T.W., Boyle, R.A., Canfield, D.E., Connelly, J.N., Gill, B.C., Lenton, T.M., Bizzarro, M., 2014. Uranium isotopes distinguish two geochemically distinct stages during the later Cambrian SPICE event. *Earth Planet. Sci. Lett.* 401, 313–326. Available at: <https://doi.org/10.1016/j.epsl.2014.05.043>.
- Dellinger, M., 2013. Apport des isotopes du lithium et des éléments alcalins à la compréhension des processus d'altération chimique et de recyclage sédimentaire. Institut de Physique du Globe de Paris.
- Dellinger, M., Gaillardet, J., Bouchez, J., Calmels, D., Galy, V., Hilton, R.G., Louvat, P., France-Lanord, C., 2014. Lithium isotopes in large rivers reveal the cannibalistic nature of modern continental weathering and erosion. *Earth Planet. Sci. Lett.* 401, 359–372.
- Dellinger, M., Gaillardet, J., Bouchez, J., Calmels, D., Louvat, P., Dosseto, A., Gorge, C., Alanoca, L., Maurice, L., 2015. Riverine Li isotope fractionation in the Amazon River basin controlled by the weathering regimes. *Geochim. Cosmochim. Acta* 164, 71–93.
- Dellinger, M., Hilton, R.G., Nowell, G.M., 2021. Fractionation of rhenium isotopes in the Mackenzie River basin during oxidative weathering. *Earth Planet. Sci. Lett.* 573, 117131. Available at: <https://doi.org/10.1016/j.epsl.2021.117131>.
- Dunk, R.M., Mills, R.A., Jenkins, W.J., 2002. A reevaluation of the oceanic uranium budget for the Holocene. *Chem. Geol.* 190, 45–67.
- Ferrier, K.L., Kirchner, J.W., 2008. Effects of physical erosion on chemical denudation rates: a numerical modeling study of soil-mantled hillslopes. *Earth Planet. Sci. Lett.* 272, 591–599.
- Gaillardet, J., Dupré, B., Allège, C.J., 1999a. Geochemistry of large river suspended sediments: Silicate weathering or recycling tracer? *Geochim. Cosmochim. Acta* 63, 4037–4051.
- Gaillardet, J., Dupré, B., Louvat, P., Allège, C.J., 1999b. Global silicate weathering and CO₂ consumption rates deduced from the chemistry of large rivers. *Chem. Geol.* 159, 3–30.
- Gislason, S.R., Arnorsson, S., Armannsson, H., Gislason, S.D.S.R., Arnórsson, S., Armannsson, H., 1996. Chemical weathering of basalt in Southwest Iceland; effects of runoff, age of rocks and vegetative/glacial cover. *Am. J. Sci.* 296, 837–907.
- Hilton, R.G., Galy, V., Gaillardet, J., Dellinger, M., Bryant, C., O'egan, M., Gröcke, D.R., Coxall, H., Bouchez, J., Calmels, D., 2015. Erosion of organic carbon in the Arctic as a geological carbon dioxide sink. *Nature* 524, 84.
- Holmden, C., Amini, M., Francois, R., 2015. Uranium isotope fractionation in Saanich Inlet: a modern analog study of a paleoredox tracer. *Geochim. Cosmochim. Acta* 153, 202–215. Available at: <https://doi.org/10.1016/j.gca.2014.11.012>.
- Horan, K., Hilton, R.G., Dellinger, M., Tipper, E., Galy, V., Calmels, D., Selby, D., Gaillardet, J., Ottley, C.J., Parsons, D.R., Burton, K.W., 2019. Carbon dioxide emissions by rock organic carbon oxidation and the net geochemical carbon budget of the Mackenzie River Basin. *Am. J. Sci.* 319, 473–499.
- Horan, K., Hilton, R.G., McCoy-West, A.J., Selby, D., Tipper, E.T., Hawley, S., Burton, K.W., 2020. Unravelling the controls on the molybdenum isotope ratios of river waters. *Geochim. Perspect. Lett.* 1–6.
- Huh, Y., Birk, J.-L., Allège, C.J., 2004. Osmium isotope geochemistry in the Mackenzie River Basin. *Earth Planet. Sci. Lett.* 222, 115–129.
- Jemison, N.E., Johnson, T.M., Shiel, A.E., Lundstrom, C.C., 2016. Uranium isotopic fractionation induced by U(VI) adsorption onto common aquifer minerals. *Environ. Sci. Technol.* 50, 12232–12240.
- Johnson, M., DePaolo, D.J., Lawrence, O., 1997. Rapid exchange effects on isotope ratios in groundwater systems. *Water Res.* 33, 187–195.
- Kendall, B., Brenneka, G.A., Weyer, S., Anbar, A.D., 2013. Uranium isotope fractionation suggests oxidative uranium mobilization at 2.50Ga. *Chem. Geol.* 362, 105–114. Available at: <https://doi.org/10.1016/j.chemgeo.2013.08.010>.
- Kendall, B., Wang, J., Zheng, W., Romaniello, S.J., Over, D.J., Bennett, Y., Xing, L., Kunert, A., Boyes, C., Liu, J., 2020. Inverse correlation between the molybdenum and uranium isotope compositions of Upper Devonian black shales caused by changes in local depositional conditions rather than global ocean redox variations. *Geochim. Cosmochim. Acta* 287, 141–164. Available at: <https://doi.org/10.1016/j.gca.2020.01.026>.
- Kipp, M.A., Li, H., Ellwood, M.J., John, S.G., Middag, R., Adkins, J.F., Tissot, F.L.H., 2022. ^{238}U , ^{235}U and ^{234}U in seawater and deep-sea corals: a high-precision reappraisal. *Geochim. Cosmochim. Acta* 336, 231–248. Available at: <https://doi.org/10.1016/j.gca.2022.09.018>.
- Langmuir, D., 1978. Uranium solution-mineral equilibria at low temperatures with applications to sedimentary ore deposits. *Geochim. Cosmochim. Acta* 42, 547–569.
- Lau, K.V., Maher, K., Altiner, D., Kelley, B.M., Kump, L.R., Lehmann, D.J., Silva-Tamayo, J.C., Weaver, K.L., Yu, M., Payne, J.L., 2016. Marine anoxia and delayed Earth system recovery after the end-Permian extinction. *Proc. Natl. Acad. Sci. U. S. A.* 113, 2360–2365.

- Lemarchand, D., Gaillardet, J., 2006. Transient features of the erosion of shales in the Mackenzie basin (Canada), evidences from boron isotopes. *Earth Planet. Sci. Lett.* 245, 174–189.
- Li, H., Tissot, F.L.H., 2023. UID: the uranium isotope database. *Chem. Geol.* 618, 121221. Available at: <https://doi.org/10.1016/j.chemgeo.2022.121221>.
- Ma, L., Chabaux, F., Pelt, E., Granet, M., Sak, P.B., Gaillardet, J., Lebedeva, M., Brantley, S.L., 2012. The effect of curvature on weathering rind formation: evidence from Uranium-series isotopes in basaltic andesite weathering clasts in Guadeloupe. *Geochim. Cosmochim. Acta* 80, 92–107. Available at: <https://doi.org/10.1016/j.gca.2011.11.038>.
- Maier, K., 2010. The dependence of chemical weathering rates on fluid residence time. *Earth Planet. Sci. Lett.* 294, 101–110.
- Maier, K., 2011. The role of fluid residence time and topographic scales in determining chemical fluxes from landscapes. *Earth Planet. Sci. Lett.* 312, 48–58.
- Millot, R., Gaillardet, J., Dupré, B., Allègre, C.J., Allègre, C.J., 2003. Northern latitude chemical weathering rates: clues from the Mackenzie River Basin, Canada. *Geochim. Cosmochim. Acta* 67, 1305–1329.
- Millot, R., Vigier, N., Gaillardet, J., 2010. Behaviour of lithium and its isotopes during weathering in the Mackenzie Basin, Canada. *Geochim. Cosmochim. Acta* 74, 3897–3912.
- Misra, S., Froelich, P.N., 2012. Lithium isotope history of Cenozoic seawater: changes in silicate weathering and reverse weathering. *Science* (80) 335, 818–823.
- Montoya-Pino, C., Weyer, S., Anbar, A.D., Pross, J., Oschmann, W., van de Schootbrugge, B., Arz, H.W., 2010. Global enhancement of ocean anoxia during oceanic anoxic event 2: a quantitative approach using U isotopes. *Geology* 38, 315–318.
- Noordmann, J., Weyer, S., Georg, R.B., Jöns, S., Sharma, M., 2016. $^{238}\text{U}/^{235}\text{U}$ isotope ratios of crustal material, rivers and products of hydrothermal alteration: new insights on the oceanic U isotope mass balance. *Isot. Environ. Health Stud.* 52, 141–163. Available at: <https://doi.org/10.1080/10256016.2015.1047449>.
- Palmer, M.R., Edmond, J.M., 1993. Uranium in river water. *Geochim. Cosmochim. Acta* 57, 4947–4955.
- Reeder, S.W., Hitchon, B., Levinson, A.A., 1972. Hydrogeochemistry of the surface waters of the Mackenzie River drainage basin, Canada? I. Factors controlling inorganic composition. *Geochim. Cosmochim. Acta* 36, 825–865.
- Romaniello, S.J., Herrmann, A.D., Anbar, A.D., 2013. Uranium concentrations and $^{238}\text{U}/^{235}\text{U}$ isotope ratios in modern carbonates from the Bahamas: Assessing a novel paleoredox proxy. *Chem. Geol.* 362, 305–316. Available at: <https://doi.org/10.1016/j.chemgeo.2013.10.002>.
- Ross, D.J.K., Bustin, R.M., 2009. Investigating the use of sedimentary geochemical proxies for paleoenvironment interpretation of thermally mature organic-rich strata: examples from the Devonian-Mississippian shales, Western Canadian Sedimentary Basin. *Chem. Geol.* 260, 1–19. Available at: <https://doi.org/10.1016/j.chemgeo.2008.10.027>.
- Rudnick, R.L., Gao, S., 2013. Composition of the continental crust. In: *Treatise on Geochemistry*, Second edition, pp. 1–51.
- Sarin, M.M., Krishnaswami, S., Somayajulu B. L. K. and Moore W. S., 1990. Chemistry of uranium, thorium, and radium isotopes in the Ganga-Brahmaputra river system: Weathering processes and fluxes to the Bay of Bengal. *Geochim. Cosmochim. Acta* 54, 1387–1396.
- Stirling, C.H., Andersen, M.B., Potter, E.K., Halliday, A.N., 2007. Low-temperature isotopic fractionation of uranium. *Earth Planet. Sci. Lett.* 264, 208–225.
- Taylor, S.R., McLennan, S.M., 1995. The geochemical evolution of the continental crust. *Rev. Geophys.* 33, 241–265.
- Telus, M., Dauphas, N., Moynier, F., Tissot, F.L.H., Teng, F.Z., Nabelek, P.I., Craddock, P. R., Groat, L.A., 2012. Iron, zinc, magnesium and uranium isotopic fractionation during continental crust differentiation: the tale from migmatites, granitoids, and pegmatites. *Geochim. Cosmochim. Acta* 97, 247–265.
- Tipper, E.T., Calmels, D., Gaillardet, J., Louvat, P., Capmas, F., Dubacq, B., 2012. Positive correlation between Li and Mg isotope ratios in the river waters of the Mackenzie Basin challenges the interpretation of apparent isotopic fractionation during weathering. *Earth Planet. Sci. Lett.* 333, 35–45.
- Tissot, F.L.H., Dauphas, N., 2015. Uranium isotopic compositions of the crust and ocean: Age corrections, U budget and global extent of modern anoxia. *Geochim. Cosmochim. Acta* 167, 113–143.
- Tribouillard, N., Algeo, T.J., Lyons, T., Riboulleau, A., 2006. Trace metals as paleoredox and paleoproductivity proxies: an update. *Chem. Geol.* 232, 12–32.
- Vigier, N., Bourdon, B., Turner, S., Allègre, C.J., 2001. Erosion timescales derived from U-decay series measurements in rivers. *Earth Planet. Sci. Lett.* 193, 549–563.
- Wang, X., Johnson, T.M., Lundstrom, C.C., 2015. Isotope fractionation during oxidation of tetravalent uranium by dissolved oxygen. *Geochim. Cosmochim. Acta* 150, 160–170. Available at: <https://doi.org/10.1016/j.gca.2014.12.007>.
- Weyer, S., Anbar, A.D., Gerdes, A., Gordon, G.W., Algeo, T.J., Boyle, E.A., 2008. Natural fractionation of $^{238}\text{U}/^{235}\text{U}$. *Geochim. Cosmochim. Acta* 72, 345–359.
- Zhou, J., Du, J., Moore, W.S., Qu, J., Zhang, G., 2015. Concentrations and fluxes of uranium in two major Chinese rivers: the Changjiang River and the Huanghe River. *Estuar. Coast. Shelf Sci.* 152, 56–64. Available at: <https://doi.org/10.1016/j.ecss.2014.11.004>.